

Cometary globules

III. Triggered star formation in IC 1848

Bertrand Lefloch^{1,2}, Bernard Lazareff³, and Alain Castets²

¹ IRAM, Avda. Divina Pastora 7, N.C., E-18012 Granada, Spain

² Laboratoire d'Astrophysique, Observatoire de Grenoble, Université Joseph Fourier, B.P. 53X, F-38041 Grenoble, France

³ IRAM, 300 Rue de la Piscine, F-38406 St. Martin d'Hères Cedex, France

Received 20 November 1996 / Accepted 31 January 1997

Abstract. We present a multiwavelength study from molecular and continuum observations of the cometary globule CG5 in the HII region IC1848. CG5 is associated with the luminous IRAS point source 02252+6120 ($L=1100 L_{\odot}$) and shows evidence for an energetic outflow and ongoing star formation (a cluster of low-mass stars has formed inside the cloud). CG5 is presently undergoing a second episode of photo-ionisation from a cluster of O stars in the nebula, characterised by a shock at the surface of the cloud; the shock was detected in several millimeter lines (CO, CS) and in the thermal continuum dust emission. Photo-ionisation conditions at the surface of the globule were estimated from measurements of the VLA free-free continuum emission. A virial analysis suggests that CG5 is probably permeated by a static magnetic field of strength $\approx 125 \mu\text{G}$ and is subject to an outer pressure 4 times as large as its inner pressure. It is in a globally magnetically subcritical state whereas its core is close to virial equilibrium. Photo-ionisation is found to play a key role in the evolution of CG5 because a) it confines the molecular gas and contains the gas dispersal favored by the energy injection from the outflow while evaporating the superficial layers at the same time, b) the overpressure of the compressed gas ahead of the ionisation front is sufficient to trigger the collapse of initially (sub)critical condensations inside the cloud and initiate star formation. We find that the outflow contains enough momentum to have contributed to this star-formation process. In addition, the energy of the outflow is sufficient to sustain turbulence in the cloud and maintain it in a magnetically subcritical state, i.e. it tends to stabilize the cloud against collapse and regulate star formation.

Key words: ISM: general – ISM: clouds – ISM: kinematics and dynamics – ISM: star formation – ISM: molecules

1. Introduction

Cometary Globules (CGs) are bright-rimmed dark clouds found in the environment of O-B stars in HII regions. They early attracted attention because they were found to be potential sites of star formation (Reipurth, 1983). There has been some evidence that indeed stars can form in these objects, either single (Duvert et al. 1990, Cernicharo et al. 1993) or multiple systems (Sugitani et al. 1995; Deharveng et al. 1996). Sugitani et al. (1991, 1994) compiled the properties of a large sample of cometary and bright-rimmed globules associated with IRAS point sources. The authors suggested that CGs would contribute efficiently to the IMF in forming low- and intermediate-mass stars. However, no systematic work benefitting from high-angular resolution molecular line studies has been undertaken so far, nor has been the peculiar birth and evolution mechanism of CGs further investigated in the process of star formation.

Previous work has shown that radiatively-driven implosion (RDI) plays a key role in the formation and evolution of cometary globules (Bertoldi 1989, 1990; Lefloch and Lazareff, 1994, 1995 – hereafter LL94 and LL95). LL94 described a dynamical model for the formation and evolution of cometary globules. Initially, the UV photons of the O stars of the nebula sweep away the low-density material, leaving the densest clumps exposed to the ionising flux. For typical ionising conditions, an ionisation front develops at the surface of the cloud. The overpressure of the ionised gas with respect to the cloud causes the ionised gas to expand freely in the interstellar medium, so that the cloud is surrounded by an ionised boundary layer (IBL), and drives a shock front in the neutral gas. This shock converges on the axis of the cloud and leads to the formation of a dense core. This short-lived collapse phase (of the order of 10^4 yr) is followed by a transient phase of re-expansion – compression before reaching a stationary quasi-stationary equilibrium, in which the cloud has developed a "head-tail" (so-called cometary) structure. This study concluded that CGs are gravitationally stable at small and large scales. LL95 reported millimeter lines observations of molecular gas structure and dynamics in the cometary

globule CG7S, and presented evidence that it is in the transient phase of dynamical compression – expansion. Because this phase is short-lived, it may be difficult to find other objects in a similar state of evolution.

In an effort to better understand the star-forming conditions in CGs, still a puzzle in the framework of RDI, and estimate the possible influence of photo-ionisation in this process, we have started a study of a wider sample of CGs, generally in the more quiescent quasi-equilibrium phase of their evolution, both in the northern and southern hemispheres. We have supplemented the molecular line observations with bolometer observations of thermal dust emission – a direct probe of the mass condensation surrounding protostellar objects – and VLA 5GHz observations of the free-free emission of the bright rim, or ionized boundary layer (IBL), – allowing a direct measurement of the boundary pressure. Our sample of objects includes: CG4, CG5, CG11B, CG13, CG34, CG37, CG43, CG51, CG87 of the list of Sugitani et al. (1991, 1994) and two globules referred as GN 00.49.9, GN 07.30.9 in the nomenclature of Neckel and Vehrenberg (1985). Here, we report on our observations of CG5, which deserves particular attention because it contains a very luminous buried IR source and a young bipolar outflow. We took the nominal coordinates of the IR source as reference position for our observations, i.e.:

$$\alpha = 02^{\text{h}}25^{\text{m}}14.5^{\text{s}} \quad \delta = 61^{\circ}20'10'' \quad (1950).$$

We will report on the observations of the other CGs in a forthcoming paper (Lefloch et al., 1997).

2. Morphology and location in Sharpless 190

CG5 is located on the West rim of the HII region IC1848, pointing inwards to a group of O stars located in the central part of the HII region: BD+60°497-499- 501-502-504-507. Following Sugitani *et al*, we adopt for IC1848 a distance of 1.9 kpc. The coordinates and Lyman-continuum luminosities of the exciting stars are listed in Table 1. Their combined Ly-c flux at the projected distance to CG5 amounts to $6.0 \cdot 10^9 \text{ cm}^{-2} \text{ s}^{-1}$, neglecting any intervening absorption. Table 1 shows that the main contribution to the ionising flux comes from stars at a declination ($61^{\circ}15'$) very close to the declination of CG5, and is almost planar at the distance of CG5 (see Fig. 1). Sugitani *et al* (1991) classify CG5 as morphological type B, i.e. of medium elongation (see Fig.1). However, the different curvatures of the north and south edges of CG5 make it asymmetric, unlike some other globules of the nebula (CG7, CG7S for instance). We also note that the main axis of CG5 does *not* point right towards the O star cluster, as shown by the arrow on Fig. 1. These facts suggest that CG5 has already experienced in the past the photo-ionisation process described in LL94, the Ly-c flux being supplied by now-extinct stars located due east. Such a situation can be expected to arise naturally in a complex evolved HII region comprising a number of O stars.

The IRAS point source 02252+6120 is located in the head of CG5. The semi-major axis of the uncertainty ellipse makes a position angle of $+61^{\circ}$ with respect to North; it is $27''$ long while the semi-minor axis is only $4''$ long. The IRAS fluxes

of the source are 9.81, 55.98, 239.51 and 638.83 at 12, 25, 60 and $100 \mu\text{m}$ respectively. Adopting the procedure described by Myers et al. (1987), we estimate a total IR luminosity $L_{\text{IR}} = 1100 L_{\odot}$. Assuming an opacity law $\kappa_{\nu} \propto \nu$ in the FIR range, we derived dust temperatures of 135, 68 and 32 K from the S_{25}/S_{12} , S_{60}/S_{25} , S_{100}/S_{60} ratios respectively.

3. Ionising conditions at the boundary of CG5

3.1. Free-free emission of a photo-ionised globule

As recalled above, the photo-ionised cloud is surrounded by a shell of ionised gas and electrons. Its effective thickness is ηR_{cloud} with $\eta \sim 0.2$ (Bertoldi, 1989). For typical ionising conditions most of the UV photons are consumed through recombinations in the shell and the ionising flux Φ can be related to the effective shell thickness ηR and the electronic density n_e using Eq. 10 of LL94: one can write:

$$\Phi_9 = \left(\frac{\Phi}{10^9 \text{ cm}^{-2} \text{ s}^{-1}} \right) \quad (1)$$

$$= 8.316 \cdot 10^{-4} \left(\frac{n_e}{1 \text{ cm}^{-3}} \right)^2 \left(\frac{\eta R}{1 \text{ pc}} \right) \quad (2)$$

so that the free-free emission measure EM of the ionised gas is:

$$EM \simeq \int_0^{\eta R} n_e^2 dl = 1.203 \cdot 10^3 \Phi_9 \text{ cm}^{-6} \text{ pc} \quad (3)$$

In the optically thin regime, the flux density S_{ν} can be written as $S_{\nu} = B_{\nu}(T_e)\tau_{\nu}\Omega_s$ (Ω_s = source solid angle). For a gaussian intensity distribution of width θ (HPFW) the source solid angle Ω_s is $2.66 \cdot 10^{-9} (\theta/10'')^2$. Using the expression of the opacity τ_{ν} for free-free emission from Mezger and Henderson (1967):

$$\tau_{\nu} \simeq 8.235 \cdot 10^{-2} \left(\frac{T_e}{1 \text{ K}} \right)^{-1.35} \left(\frac{\nu}{1 \text{ GHz}} \right)^{-2.1} \left(\frac{EM}{1 \text{ pc cm}^{-6}} \right)$$

one derives the following relations for the Rayleigh-Jeans brightness temperature and the flux S_{ν} :

$$\left(\frac{T_B}{1 \text{ K}} \right) = 3.942 \left(\frac{T_e}{10^4 \text{ K}} \right)^{-0.35} \left(\frac{\nu}{1 \text{ GHz}} \right)^{-2.1} \Phi_9 \quad (4)$$

$$\left(\frac{S_{\nu}}{1 \text{ mJy}} \right) = 0.321 \Phi_9 \left(\frac{T_e}{10^4 \text{ K}} \right)^{-0.35} \left(\frac{\nu}{1 \text{ GHz}} \right)^{-0.1} \quad (5)$$

$$\times \left(\frac{\theta}{10''} \right)^2 \quad (6)$$

3.2. Observations

The observations of the free-free emission in the bright rim of CG5 were carried out with the VLA of NRAO¹ in May 1995.

¹ The National Radio Astronomy Observatory is operated by Associated Universities, Inc., under cooperative agreement with the National Science Foundation.

Table 1. Coordinates, Spectral type, Ly-c Luminosity and Ly-c Flux of the ionising stars neighbouring CG5.

BD	R.A.	DEC	Sp	$\log(L_i/1 \text{ s}^{-1})$	$F_i (\text{cm}^{-2} \text{ s}^{-1})$
+60°493	02 ^h 27 ^m 04.4 ^s	60°57'22"	B0.5Ia	47.60	1.57 10 ⁷
+60°497	02 ^h 28 ^m 08.4 ^s	61°23'29"	O7	48.62	2.54 10 ⁸
+60°501	02 ^h 28 ^m 47.8 ^s	61°15'12"	O6.5	48.82	2.64 10 ⁸
+60°499	02 ^h 28 ^m 28.1 ^s	61°19'57"	O9.5V	47.84	3.49 10 ⁷
+60°502	02 ^h 28 ^m 53.9 ^s	61°14'09"	O5e	49.62	1.55 10 ⁹
+60°504	02 ^h 29 ^m 01.1 ^s	61°09'30"	O4	49.93	2.71 10 ⁹
+60°507	02 ^h 29 ^m 31.5 ^s	61°18'07"	O5e	49.62	1.19 10 ⁹

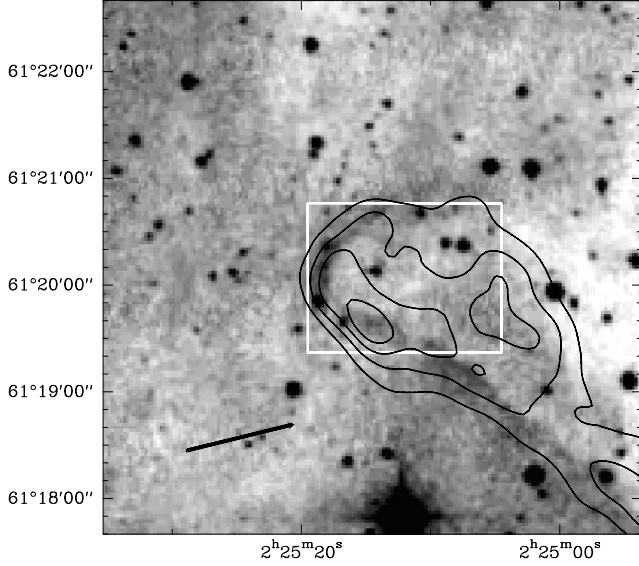


Fig. 1. Contour map of the free-free emission measured at 6cm overlaid on a red POSS image of CG5. First level and contour interval are 1.5 mJy/beam. The white box delineates the region observed in molecular tracers. The arrow shows the direction of the mean flux of Ly-c photons from the stars listed in Table 1, assumed to lie in the plane of the sky.

We used the quasars 0134 + 329 as primary and 2145 + 068 and 0224 + 671 as secondary calibrators. The array was in D configuration; at the observing frequency of 5 GHz we obtained a synthesized beam of 14". The data were reduced using the standard VLA data reduction package. An rms of ≈ 0.5 mJy/beam was achieved throughout the map.

Fig. 1 shows a good coincidence between the optical morphology and the shape traced by the high-level contours (≥ 1.5 mJy/beam). The maximum emission (≈ 6.5 mJy/beam) lies on the south eastern boundary of the cloud at (+4", -30") with respect to the IRAS source, in agreement with the direction of the incoming flux (see Sect. 2). Low-level emission covers the whole surface of the cloud. It is however more extended on the southern side, following the optical boundary until $\alpha \simeq 02^{\text{h}}25^{\text{m}}45^{\text{s}}$.

3.3. Quantitative analysis

In the following we adopt $T_e = 10^4$ K. From Eq. 2 – 6, we express the effective ionising flux and the mean electronic density at the surface of the cloud:

$$\Phi_9 = 3.66 \left(\frac{S_\nu}{1 \text{ mJy}} \right) \left(\frac{\theta}{10''} \right)^{-2} \quad (7)$$

$$\left(\frac{n_e}{10^2 \text{ cm}^{-3}} \right) = 1.48 \left(\frac{S_\nu}{1 \text{ mJy}} \right)^{0.5} \left(\frac{\theta}{10''} \right)^{-1} \left(\frac{\eta R}{1 \text{ pc}} \right)^{-0.5} \quad (8)$$

We integrated the flux over the region of molecular gas fully covered by the free-free emission (i.e. the main body of CG5), leaving aside the SW wing. The size of the region covered is 103"; the critical electronic density n_c above which an ionised shell develops around the cloud is $n_c = 25 \text{ cm}^{-3}$ (see Eq. 10 of LL94). After deconvolving from the beam (14"), we get a total integrated flux $S_\nu = 139$ mJy. Thus, we infer the ionising flux at the surface of CG5 from Eq. 7 and the electronic surface density from Eq. 8

$$\Phi = 4.8 10^9 \text{ cm}^{-2} \text{ s}^{-1}$$

$$n_e = 720 \text{ cm}^{-3}$$

The electronic density n_e is much larger than n_c , fully consistent with the initial hypothesis. The effective ionising flux Φ derived at the surface of CG5 agrees quite well with our estimate in Sect. 2 although it is slightly weaker. This suggests that: a) geometrical effects are negligible (the projected distances of the illuminating sources are close to the "true" -unprojected- ones); b) the absorption of UV photons between the stars and the globule is very low; this is indirectly confirmed by the R POSS print of the HII region (see Fig 1) which exhibits only low-brightness gas between the O stars cluster and CG5.

For these ionisation conditions, a D-critical ionisation front (IF) preceded by a shock –assumed to be isothermal, see LL94– propagates from the surface into the molecular gas. The balance of dynamical pressure between ionised and neutral gas enables to derive an estimate of the density n_s in the shock. In the frame of the IF, the ionised gas leaves the surface at the sonic velocity c_i , while the velocity of the molecular gas is subsonic ($= c_n^2/(2c_i) \ll c_n$). Using "obvious" notations, the pressure balance reduces to

$$P_{ext} = 2\rho_i c_i^2 = \rho_c c_n^2 = n_s k_B T_n = 4.2 10^{-9} \text{ erg cm}^{-3} \quad (9)$$

where the temperature T_n of the surface molecular gas is close to 40 K (see Sect. 4.1). We obtain a typical density $n_s \approx 8 \cdot 10^5 \text{ cm}^{-3}$ in the compressed layer.

4. Structure of molecular gas

The observations were performed with the IRAM 30m telescope on Pico Veleta (Spain) in November 1994. We used three SIS receivers simultaneously in the 3mm, 2mm, and 1.3mm bands, together with filterbanks and autocorrelator backends. The spectral resolution (20kHz at 3mm and 2mm and 40kHz at 1.3mm) was afterwards degraded to obtain the same kinematic resolution of about 0.1 km s^{-1} for all lines. The receivers were tuned to reject the image sideband, between 10dB (1.3mm and 2mm) and 30dB (3mm). The co-alignment was checked against planets and found to lie within $2''$. Typical beamsizes are $22''$ and $11''$ for the CO, ^{13}CO and C^{18}O lines at 3mm and 1.3mm respectively, $24''$ for CS(2-1) and $\text{C}^{34}\text{S}(2-1)$, $16''$ for CS(3-2) and $\text{C}^{34}\text{S}(3-2)$, $10''$ for CS(5-4). The calibration scale was checked against standard astronomical line sources (Mauersberger *et al* 1989), and the observed spectra were converted to the T_{mb} scale, using standard main beam efficiencies (IRAM Newsletter no 19, Nov. 1995). Typical system temperatures were found to be 250 – 300 K, 350 – 500 K and 350 – 700 K at 3mm, 2mm and 1.3mm respectively. Pointing was checked approximately every two hours on W3OH; offsets corrections were always less than $3''$.

As appears below, the different tracers reveal a core-envelope density structure for the globule, whose physical properties were derived from a LVG analysis. To do so, the resolution of the upper line was first degraded to the lower transition in order to get the same spatial resolution. At each studied position, we adopted a mean linewidth close or equal of the linewidth of the main gas component. The physical properties of CG5 are summarised in Table 5.

4.1. The $^{12}\text{CO}(2-1)$ data

Fig. 2 shows the contours of integrated line intensity of $^{12}\text{CO}(2-1)$ overlaid on the optical image (POSS red image). Not surprisingly, this optically thick line traces the overall extent of the globule, in agreement with the optical image. The width of the $^{12}\text{CO}(2-1)$ at half-intensity is $65''$, corresponding to 0.6pc at the adopted distance of IC1848. The peak line temperature varies little over the whole body of the globule, between 30 K and 40 K, with the higher values on the southern side of the main axis presumably because of enhanced heating of dust in the outer layers of the globule, as suggested by the good overlap between the regions of maximum T_{mb} and of maximum free-free emission, also observed in the $\text{C}^{18}\text{O}(2-1)$ and $^{13}\text{CO}(2-1)$ lines (see Fig. 4).

Fig. 5 shows a velocity-channel map of the $^{12}\text{CO}(2-1)$ emission. The molecular gas emission is comprised mainly between -53 and -50 km s^{-1} , with a mean velocity centered at -51 km s^{-1} . The velocity in the extreme head varies between

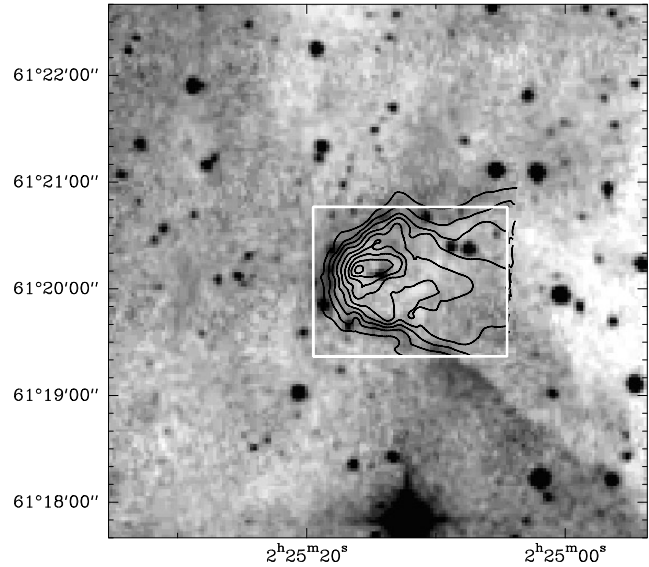


Fig. 2. Contour map of the $^{12}\text{CO}(2-1)$ integrated area on a red POSS image of CG5. First level and contour interval are 20 K km s^{-1} . The mapped area is delineated by the white box.

-53 and -52 km s^{-1} , shifted with respect to the velocity of the main body gas.

Prominent red and/or blue wings are apparent in the vicinity of the IRAS point source. These wings are distributed as two well separated lobes, characteristic of a bipolar outflow, which will be discussed separately. Besides this double-lobe structure, the red wing shows an elongated extension to the south-west, along the south edge of CG5. The morphology of the region of redshifted gas looks very similar to the free-free continuum emission map (compare Fig. 1 and the $^{12}\text{CO}(2-1)$ emission at $v = -49 \text{ km s}^{-1}$ on Fig. 5). This extension correlates well with the local enhancement of brightness observed in the optically thick $^{12}\text{CO}(2-1)$ line as well as its isotopomers $^{13}\text{CO}(2-1)$ and $\text{C}^{18}\text{O}(2-1)$ (see Fig. 4) and probably traces the compression of the surface gas of the southern edge, illuminated and photoionised by the O star cluster. This is one of the very few evidences of compression induced by photo-evaporation observed until now.

4.2. The ^{13}CO data

The ^{13}CO emission extends over more than $100''$ along the major axis and $60''$ along the minor axis of CG5. We define the ^{13}CO clump from the contour level at 30% in the integrated area map of the optically thin (1-0) transition (see Fig. 3): this contour covers approximately the whole molecular condensation while leaving aside the diffuse outer layers. The clump makes a P.A. of $+60^\circ$ (it is therefore aligned along the major axis of CG5). It has a flattened shape of dimensions $0.90 \times 0.52 \text{ pc}$ (major and minor axis respectively). It appears to peak slightly ahead of the IRAS source.

We took a mean kinetic temperature $T_k = 30 \text{ K}$, except around the (0,0) position where we adopted $T_k = 40 \text{ K}$,

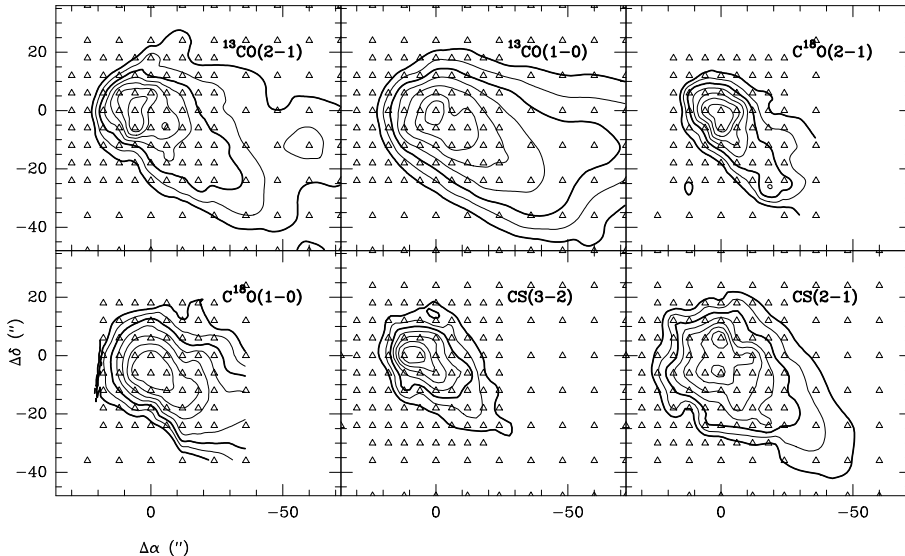


Fig. 3. Integrated area emission maps in the $^{13}\text{CO}(2-1)$, $^{13}\text{CO}(1-0)$, $\text{C}^{18}\text{O}(2-1)$, $\text{C}^{18}\text{O}(1-0)$, $\text{CS}(3-2)$ and $\text{CS}(2-1)$ lines. Contours levels are 30, 40, 50, ..., 90 % of the integrated area peak. Thick contours trace the levels at 30% and 50%.

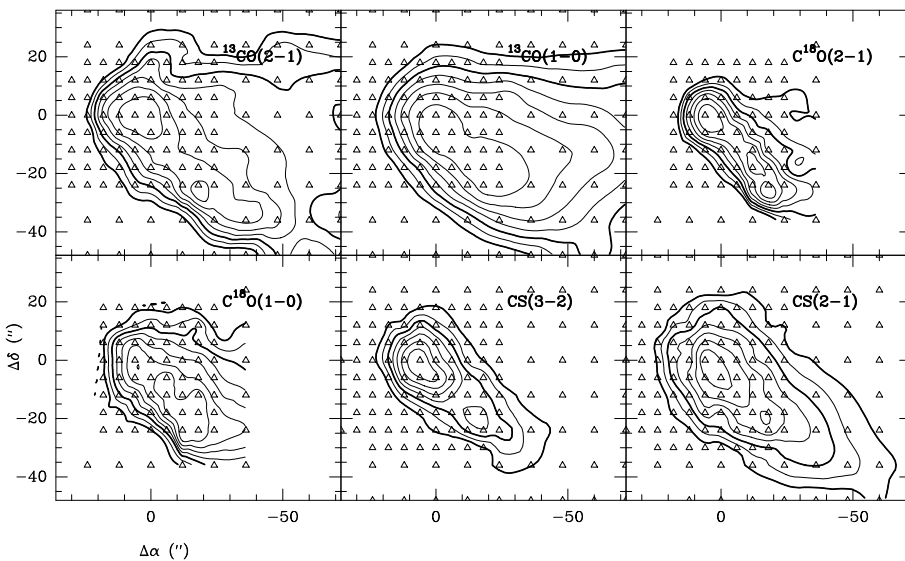


Fig. 4. Main-Beam brightness temperature maps in the $^{13}\text{CO}(2-1)$, $^{13}\text{CO}(1-0)$, $\text{C}^{18}\text{O}(2-1)$, $\text{C}^{18}\text{O}(1-0)$, $\text{CS}(3-2)$, and $\text{CS}(2-1)$ lines. Contours levels are 30, 40, 50, ..., 90 % of the brightness peak. Thick contours trace the levels at 30% and 50%. Maximum brightness temperatures for each transition are marked at the upper left corner of the maps.

in agreement with the C^{18}O observations (see Sect. 4.3) and a mean linewidth $\Delta v = 2.1 \text{ km s}^{-1}$. The column density is relatively uniform over the cloud, with an average value $N(\text{H}_2) = 3.0 \cdot 10^{22} \text{ cm}^{-2}$ assuming an abundance $\chi(^{13}\text{CO}) = [^{13}\text{CO}]/[\text{H}_2] = 1.6 \cdot 10^{-6}$. Because the (2-1) and (1-0) transitions are close to thermal equilibrium, density determinations from excitation calculations suffer large uncertainties; instead, densities were derived from column density under the assumption of cylindrical geometry. We found a mean H_2 density $n(\text{H}_2) = 3.9 \cdot 10^4 \text{ cm}^{-3}$. The $^{13}\text{CO}(2-1)$ line is moderately optically thick ($\langle \tau^{21} \rangle = 1.6$) whereas the $^{13}\text{CO}(1-0)$ is optically thin ($\langle \tau^{10} \rangle = 0.49$). We infer a mass of $135 M_\odot$.

4.3. The C^{18}O data

The $\text{C}^{18}\text{O}(2-1)$ and (1-0) lines were observed on a square grid of size $42''$ with a $6''$ spacing (Nyquist-sampling at the $\text{C}^{18}\text{O}(2-1)$ frequency) centered on the head of CG5. The C^{18}O emission

shows a clump approximately circular of $20''$ diameter centered at (0,-3) prolonged by a SW extension. The dimensions of this condensation are $0.48 \text{ pc} \times 0.18 \text{ pc}$ (emission at FWHP). In the following, we concentrate on the central core. The brightness temperature is relatively uniform over the cloud in the (1-0) transition while the (2-1) transition appears brighter in the SW extension of the clump. However, as will be discussed later, the south-western tail is very likely to be associated with surface gas (see Sect. 7.1).

We derived the mean C^{18}O excitation temperatures across the cloud under the assumption that the C^{18}O lines are optically thin and that both lines have the same excitation temperature. This hypothesis was verified a posteriori (see below). A map of the temperatures derived at all the observed positions is shown on Fig. 6.

The excitation temperatures appear to vary between 11 K and 52 K. The average value is: $T = 30 \text{ K}$, which we adopted as kinetic temperature for the main body gas in the rest of the

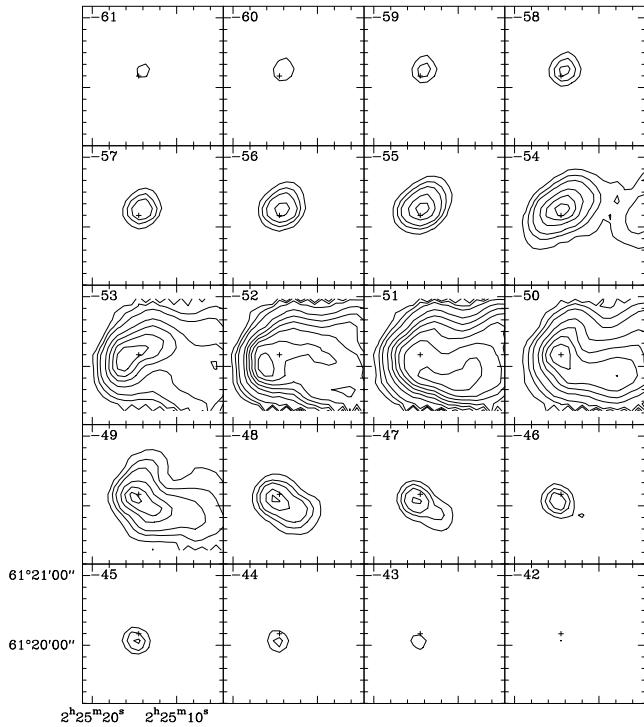


Fig. 5. Velocity channel map of the $^{12}\text{CO}(2-1)$ emission. Velocity step is 0.3 km s^{-1} ; first contours and contour interval are 1.5, 3, 5 K and 5 K respectively.

article. Fig. 6 shows a *local increase* of the kinetic temperature near the IRAS source, with a maximum located at its nominal position. Moreover, the temperature of the gas close to IRAS 02252+6120 is noticeably higher (around 50 K) than the dust temperature deduced from the S_{100}/S_{60} ratio. This strongly suggests that the molecular gas surrounding IRAS 02252+6120 is heated by the central source.

In the following we adopt 40 K as kinetic temperature for the C^{18}O condensation. We first estimated the H_2 column density by means of LVG calculations. Typical linewidths are $\Delta v = 1.0 - 1.5 \text{ km s}^{-1}$. We get an average column density $N(\text{H}_2) = 2.8 \cdot 10^{22} \text{ cm}^{-2}$, very close to the value inferred in the optically thin regime, assuming the levels populated at LTE: $N(\text{H}_2) = 3.1 \cdot 10^{22} \text{ cm}^{-2}$. Hence the mass of the C^{18}O core: $M = 21 M_{\odot}$. Under the assumption of spherical geometry the mean core density is $\langle n(\text{H}_2) \rangle = 6.7 \cdot 10^4 \text{ cm}^{-3}$. We derive mean opacities $\langle \tau^{21} \rangle = 0.17$ and $\langle \tau^{10} \rangle = 0.04$, consistent with the initial hypothesis. We could check that the excitation temperature of the lines is very close to the kinetic temperature: $T_{ex}^{10} \sim 40 \text{ K}$ and $T_{ex}^{21} \sim 36 - 38 \text{ K}$. The results of our analysis at a few typical positions in the clump are shown in Table 2.

4.4. The CS and C^{34}S data

CG5 was mapped in the CS(2-1), CS(3-2) lines, and in CS(5-4) on a smaller grid centered on the (0,0) position. Both CS(2-1) and CS(3-2) trace an elongated clump of dimensions $80'' \times 40''$ ($0.74 \times 0.37 \text{ pc}$) which peaks east of the IRAS source, there-

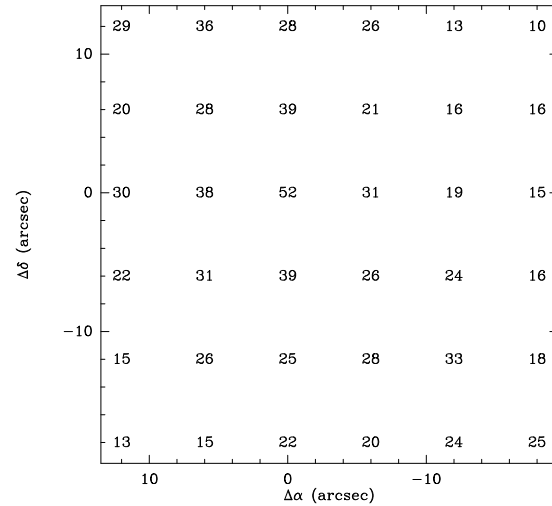


Fig. 6. Kinetic temperatures calculated from the ratio of the optically thin lines $\text{C}^{18}\text{O}(2-1)/\text{C}^{18}\text{O}(1-0)$ in the inner part of CG5 head, T_k increases near the position of the protostellar object IRAS 02252+6120.

fore resolved in all three transitions. The CS clump is made of a round condensation centered at (6,0), prolonged by a bright SW tail (see Fig. 4) of lower brightness and integrated area. We define the core of the CS(3-2) clump by taking the contour at half power (6 K km s^{-1}) of the (3-2) integrated area emission: the dimensions of the core are $0.16 \times 0.28 \text{ pc}$ (see Fig. 3). The emission of the dense gas in the core, as traced by CS, is displaced $6-12''$ ahead of the C^{18}O emission.

The physical properties of the core were derived from the CS(3-2) and the CS(2-1) lines assuming a kinetic temperature of 40 K. The results are summarised in Table 3. The densities and the column densities appear relatively uniform over the core, with typical values: $n(\text{H}_2) = 1.5 \cdot 10^5 \text{ cm}^{-3}$, $N(\text{H}_2) = 5 \cdot 10^{21} \text{ cm}^{-2}$, assuming a standard abundance $\chi(\text{CS}) = 5.0 \cdot 10^{-9}$. These results agree well with the analysis of from the $\text{C}^{34}\text{S}(3-2)$ and (2-1) lines, from which H_2 densities $\approx 2 - 4 \cdot 10^5 \text{ cm}^{-3}$. The core is moderately optically thin: $\langle \tau^{32} \rangle = 0.7$, and $\langle \tau^{21} \rangle = 0.35$. The density slightly increases around the (0,0) position, an effect more apparent at higher angular resolution. From the analysis of (5-4) and (3-2) at a few positions, we find the density to be strongly peaked at the (0,0) and (0,-6) offset positions: $n(\text{H}_2) = 1.5 \cdot 10^6 \text{ cm}^{-3}$. From the mean H_2 density, we estimate the mass of the core: $M = 18 M_{\odot}$.

The presence of a star cluster associated with the IRAS source (see below) indicates a clumpy structure in the densest parts of the globule. However, the core was resolved not only in the CS lines but also in the optically thin $\text{C}^{34}\text{S}(3-2)$ line. The ratio of CS to C^{34}S in the (2-1) and (3-2) transitions is ≈ 10 in the core, not very different from the values expected in the absence of clumpiness (14–20) assuming a relative abundance $\text{CS}/\text{C}^{34}\text{S}$ of 20. Therefore, strong clumping of the core can be excluded and it is unlikely that “exotic” radiative transfer effects, such as e.g. radiative scattering, play an important role in the core

Table 2. Physical properties of the $C^{18}O$ clump at a few observed positions, as derived from the LVG analysis. Densities are calculated from column densities assuming spherical symmetry.

offsets	T_{MB}^{10} (K)	Δv^{10} (km s $^{-1}$)	T_{MB}^{21} (K)	Δv^{21} (km s $^{-1}$)	$N(C^{18}O)$ (cm $^{-2}$)	$n(H_2)$ (cm $^{-3}$)	τ^{10}	τ^{21}
(-12,-12)	2.0	1.5	6.0	1.3	$6.0 \cdot 10^{15}$	$7.9 \cdot 10^4$	0.06	0.21
(-6,-6)	2.2	1.5	5.9	1.5	$5.4 \cdot 10^{15}$	$7.7 \cdot 10^4$	0.05	0.17
(-6,6)	1.5	1.5	3.6	1.6	$3.1 \cdot 10^{15}$	$4.1 \cdot 10^4$	0.03	0.10
(0,-6)	2.0	1.5	6.3	1.6	$7.2 \cdot 10^{15}$	$9.5 \cdot 10^4$	0.06	0.20
(0,6)	1.5	1.6	4.7	1.5	$7.1 \cdot 10^{15}$	$9.3 \cdot 10^4$	0.06	0.20
(6,-6)	2.0	1.6	5.7	1.3	$6.0 \cdot 10^{15}$	$7.9 \cdot 10^4$	0.06	0.21
(6,6)	1.8	1.4	4.9	1.6	$4.4 \cdot 10^{15}$	$5.7 \cdot 10^4$	0.04	0.14
(12,0)	1.5	1.4	4.3	1.3	$4.2 \cdot 10^{15}$	$5.5 \cdot 10^4$	0.04	0.15

Table 3. LVG analysis of the CS core from the CS(3-2) and (2-1) lines.

offsets	T_{MB}^{21} (K)	T_{MB}^{32} (K)	$\langle \Delta v \rangle$ (km s $^{-1}$)	$n(H_2)$ (cm $^{-3}$)	$N(CS)$ (cm $^{-2}$)	τ^{21}	τ^{32}
(-12,-24)	3.0	2.3	1.3	$1.0 \cdot 10^5$	$2.4 \cdot 10^{13}$	0.50	0.83
(-12,0)	2.8	2.6	1.8	$1.7 \cdot 10^5$	$1.9 \cdot 10^{13}$	0.27	0.56
(-12,12)	1.8	1.5	2.0	$1.2 \cdot 10^5$	$1.3 \cdot 10^{13}$	0.25	0.45
(-6,-6)	3.8	3.6	1.7	$1.8 \cdot 10^5$	$2.4 \cdot 10^{13}$	0.33	0.73
(-6,6)	3.1	2.8	1.8	$1.6 \cdot 10^5$	$2.2 \cdot 10^{13}$	0.31	0.65
(0,-24)	2.1	1.7	1.6	$1.1 \cdot 10^5$	$1.5 \cdot 10^{13}$	0.31	0.53
(0,-12)	3.7	3.5	1.6	$1.7 \cdot 10^5$	$2.8 \cdot 10^{13}$	0.34	0.75
(0,0)	4.0	4.1	1.6	$2.2 \cdot 10^5$	$3.0 \cdot 10^{13}$	0.28	0.70
(0,12)	2.5	2.5	1.6	$2.1 \cdot 10^5$	$1.7 \cdot 10^{13}$	0.18	0.45
(6,-6)	3.9	4.0	1.6	$2.1 \cdot 10^5$	$3.0 \cdot 10^{13}$	0.30	0.71
(6,6)	3.6	3.7	1.7	$2.1 \cdot 10^5$	$2.6 \cdot 10^{13}$	0.26	0.64
(12,-24)	1.3	0.9	1.9	$9.3 \cdot 10^4$	$8.9 \cdot 10^{12}$	0.22	0.34
(12,0)	2.9	3.6	1.7	$3.8 \cdot 10^5$	$2.0 \cdot 10^{13}$	0.11	0.36

of CG5. The quantities derived here represent reasonably good estimates of the physical conditions inside the core.

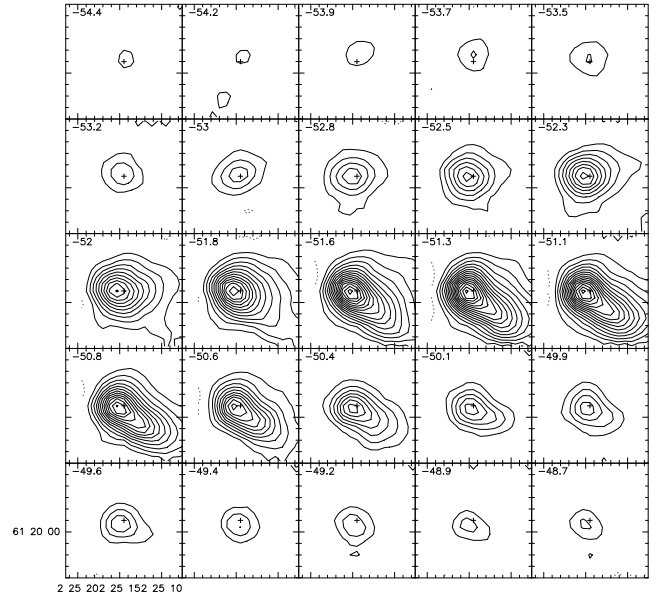
The CS clump is rather quiescent, unlike the gas of the envelope traced by ^{13}CO and ^{12}CO : the velocity channel map (see Fig. 7) shows little variation in the kinematics of the gas. The velocity of the main body gas varies between -50.5 and -52.5 km s $^{-1}$, and peaks around -51.3 km s $^{-1}$. Ambient gas draws a clump of $\approx 30''$ diameter, with a redshifted SW extension ranging from -51.6 to -50 km s $^{-1}$. At higher velocities can be seen the blue and red wings.

5. Bipolar outflow

5.1. The CO outflow

5.1.1. Morphology

We have searched for high velocity wings around IRAS 02252+6120 and have detected a small outflow. Fig. 8 shows the $^{12}CO(2-1)$ emission of the outflow, observed at 3 different positions. The wings extend from -66 km s $^{-1}$ to -41 km s $^{-1}$ (above $3\sigma = 0.6$ K, see Fig. 9).

**Fig. 7.** CS(3-2) velocity channel map. Velocity interval is 0.2 km s $^{-1}$, first contour and contour step are 0.2 K.

The mean velocity of the ambient gas (v_{lsr}) is -51 km s $^{-1}$ so that the terminal velocity of the blue and the red wings are 15 km s $^{-1}$ and 10 km s $^{-1}$ respectively.

The major axis of the outflow lies at a P.A. of -30° (see Fig. 12): it is therefore oriented perpendicular to the major axis of the (flattened) core of CG5. The emission of the high-velocity gas extends over $\approx 50''$ (i.e. \approx the whole width of the globule) and is relatively poorly collimated (collimation ratio = 1.8). The blue wing extends over $\approx 30''$ while the red one is only $20''$ long. Note however that some confusion exist between the emissions of the outflow red wing and of the compressed surface gas and that the contours of the red wing area closely follow the border of the cloud (see Fig. 5 and Fig. 10). Interestingly, the highest-velocity gas emission is concentrated around the IRAS source, and appears surrounded by lower-velocity gas emission. This agrees with the idea that CO actually traces molecular gas entrained by a faster (highly collimated) jet (Bachiller et al., 1992)

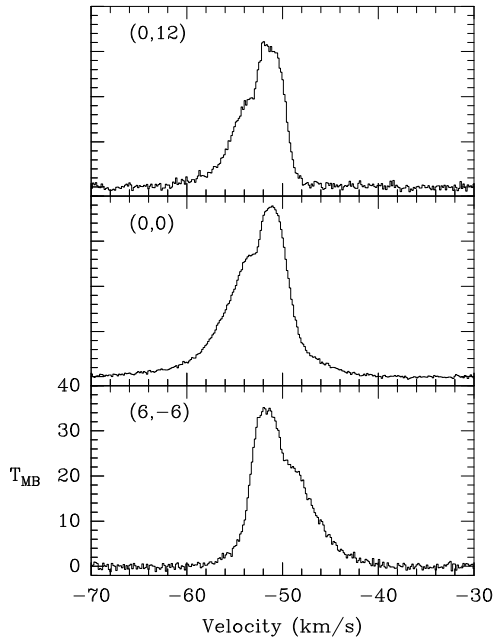


Fig. 8. Emission of the outflow in the $^{12}\text{CO}(2-1)$ line observed at three position; the offsets for each spectrum are in arcsec, relative to the nominal position of IRAS 02252+6120. The high-velocity wings, spatially well separated, extend up to 15 km s^{-1} with respect to the ambient gas velocity.

The weak overlap between both components suggest that the angle of sight is close to the opening angle of the flow, with a typical value probably closer to 90° than to 0° for the latter. From this overlap, we estimate the approximate center of the outflow to be at the offset position (0,-2), very close to the nominal position of IRAS 02252+6120, and coinciding with the CS density peak (see Sect. 4.4) confirming the former to be the powering source of the outflow. We computed the (emission-weighted) position of the velocity centroid for each wing and found the following positions: (-3,5.5) and (4,-9) for the blue and the red wings respectively. Both are very close to the center of the flow, which, despite the unknown inclination angle of the outflow, suggests a young kinematical age. We determined the radius of each lobe as the distance of the velocity centroid to the apparent outflow center. We found a mean radius of $\approx 8'' = 0.074 \text{ pc}$ over the sky.

5.2. Physical parameters of the outflow

In the following, we derive estimates of mass, momentum, energy and mechanical power for the high-velocity gas. We did not attempt to correct for projection effects which can severely affect these values (Cabrit and Bertout, 1990). Another source of error concerns the estimates of mass: the extended emission of the redshifted compressed gas cannot be readily separated from the emission of the outflow. However, since most of the latter lies below 30 K km s^{-1} (see Fig. 10), we chose this contour to delineate the extent of the red wing. In this respect, the values

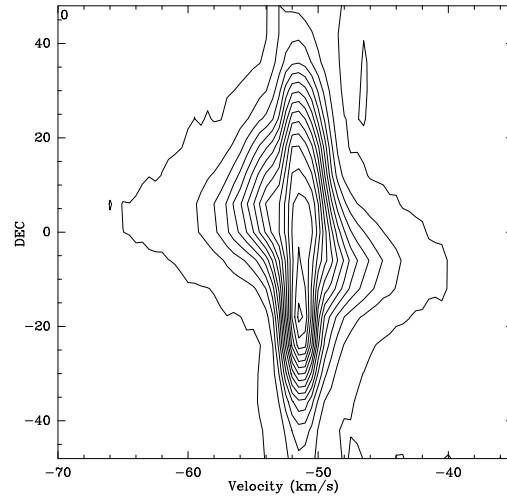


Fig. 9. Velocity-position cut of the $^{12}\text{CO}(2-1)$ emission made along the main axis of the outflow. First contour is 0.6K (3σ) and contour interval is 2.5K

derived for the mass, momentum, etc... should be regarded as lower estimates.

The mass of gas contained in each wing was estimated under the assumption that the ^{12}CO levels are populated in LTE at the excitation temperature $T_{ex} = T_k = 30 \text{ K}$. The masses were calculated in the optically thin limit before correcting for the opacity of the wings. From the $^{12}\text{CO}(2-1)/^{13}\text{CO}(2-1)$ ratio, we inferred an opacity (averaged over the wing width) of $\tau_B = 3.2$ and $\tau_R = 5.7$ for the blue and the red wing respectively. In Table 4 are summarised the mass of each wing and the other parameters of the outflow.

We derive the other dynamical parameters by first calculating the mean velocity of each wing. We found $\bar{V} = -56$ and -46 km s^{-1} , which means that both wings have the same mean velocity with respect to the gas rest velocity ($v_{lsr} = -51 \text{ km s}^{-1}$). We estimated the dynamical timescale from the ratio of the lobe size to the wing terminal velocity. We infer dynamical timescales of the order of $1.5 \cdot 10^4 \text{ yr}$. The mass loss rate was calculated assuming the outflow to be momentum conserving.

5.3. The CS emission

Blue and red wings were detected in the CS(2-1), CS(3-2) and CS(5-4) lines. These wings are more compact than in CO lines (see Fig. 11), and they overlap strongly (which may be caused by the finite resolution). The centroid and position angle of the CS wings agree well with those found for CO. A lower limit for the H_2 density in the wings can be deduced from the value of $R = T_{mb}(\text{CS}(3-2))/T_{mb}(\text{CS}(2-1))$. We find that, at the (0,0) position, $R \geq 1.3$ at all velocities. This means that $n(\text{H}_2) \geq 3 \cdot 10^5 \text{ cm}^{-3}$ assuming $T_k = 40 \text{ K}$ (and a higher limit for lower temperatures). The properties of the gas traced by the CS wings – compactness, high density, position and orientation – strongly suggest that it is primary or entrained gas near the source of the outflow.

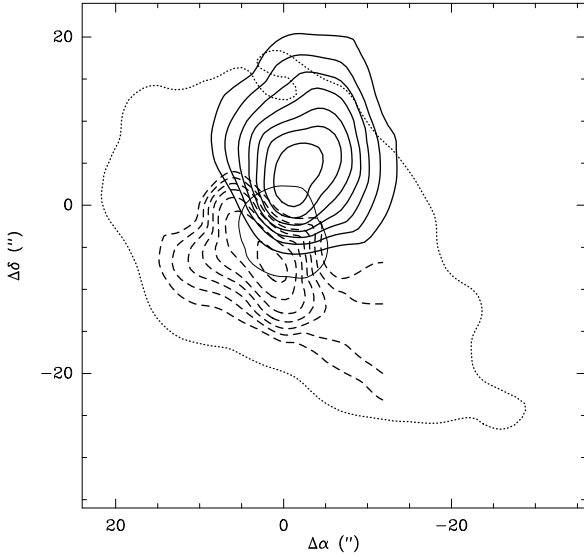


Fig. 10. Contours of integrated area for the blue (solid) and red (dashed) CO high-velocity wings. Level spacing is 10 K km s^{-1} , first contour is 20 K km s^{-1} . The dotted line delineates the CS clump; the solid contour delineates the central core.

Table 4. Physical parameters of the blue and the red wings of the outflow: mass, mean velocity, momentum, mechanical energy, dynamical timescale, mass-loss rate and mechanical power (in brackets are given the values in the optically thin limit).

	Red	Blue	Total
Size (pc)	0.14	0.28	
Mean opacity	5.7	3.2	
Mass (M_{\odot})	1.04 (.18)	.94 (.28)	2.0 (.46)
\bar{V} (km s^{-1})	-46	-56	
\bar{P} ($M_{\odot} \text{ km s}^{-1}$)	5.3 (.92)	4.6 (1.38)	
\bar{E} (10^{44} erg)	2.6 (.45)	2.4 (.72)	5.0 (1.2)
T_d (yr)	$1.2 \cdot 10^4$	$1.8 \cdot 10^4$	
\dot{M} ($10^{-5} M_{\odot} \text{ yr}^{-1}$)	4.4 (.77)	1.7 (.51)	6.1 (1.3)
\bar{L} (L_{\odot})	.18 (.032)	.11 (.033)	.29 (.065)

6. Thermal dust emission

The observations at $\lambda = 1.25\text{mm}$ were carried out at the IRAM-30m telescope with the MPIfR 19-channel bolometer in March 1995. Weather conditions were rather poor but stable: the mean sky opacity τ was ~ 0.3 over the session. The channels of the array are located at the center and on the sides of two concentric hexagons, two adjacent channels being separated by $20''$. The 19 channels have similar sensitivities apart from channel 6, whose data were discarded. Their beamwidth is $11''$ wide (HPFW) and therefore very close to the synthesized beam of the VLA observations. The source was scanned in the azimuth direction by moving the telescope at a speed of $4''/\text{sec}$; subsequent azimuth scans were spaced by $4''$ in elevation. Two maps of CG5 were made: skydips were performed before and after each map. Calibration was checked on Mars and W3(OH). The

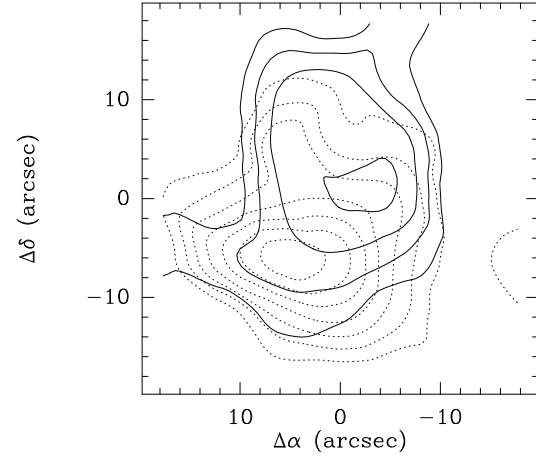


Fig. 11. Contours of integrated area emission in the CS(3-2) high-velocity wings. Solid and dashed contours are used for the blue and the red wing respectively. First contour and contour interval is 0.5 K km s^{-1} .

data were reduced and analysed with the NIC software developed by IRAM. Combining the two maps yielded an rms of $\approx 5 \text{ mJy/beam}$ in the resulting final map.

The continuum emission appears extended, with a general orientation similar to the molecular gas distribution, and traces an ellipsoidal condensation of dimensions $21'' \times 18''$ at half power (100 mJy), or $18'' \times 14''$ ($0.16 \times 0.13 \text{ pc}$) after deconvolution from the beam, very similar to the C^{18}O core (see Fig. 12). This clump is therefore resolved at 1.25mm . The emission peaks at $(0, -3)$: $F_{\text{peak}} = 200 \text{ mJy/beam}$. Like the C^{18}O emission map, this core is prolonged by a SW low-emission extension ($\leq 60 \text{ mJy/b}$).

Eq. 6 shows that the free-free emission flux from the ionised shell surrounding cometary globules depends very weakly on the frequency. Hence, at the same angular resolution, the free-free radiation contributes negligibly to the millimeter continuum emission compared with the thermal dust emission. We assumed a solar metallicity and dust absorption cross sections typical of moderately dense molecular gas: $\sigma_{\lambda}^H = 1.4 \cdot 10^{-20} (\lambda / (1\mu))^{-2}$ (see Mezger et al. 1990). After deconvolving the source from the beam (taken to be gaussian and $11''$ wide at FWHP), we get a total integrated flux of 316 mJy, using Eq. A9b–10b from Mezger et al. (1990). Adopting $T_k = 40 \text{ K}$, we derive a hydrogen column density $N(\text{H}_2) = 2.9 \cdot 10^{22} \text{ cm}^{-2}$ and a mass $M_c = 20 M_{\odot}$. These results agree very well with the C^{18}O analysis.

We can note that the H_2 surface densities derived from ^{13}CO , C^{18}O , and dust agree closely, while the length and mass scales are significantly different. This suggests, at least in the range $0.1\text{--}0.2 \text{ pc}$, a $\rho \propto r^{-1}$ mass distribution.

Table 5. Physical properties of CG5

Distance	1.9 kpc
Proj. radius	0.3 pc
Proj. size (^{13}CO)	0.9 pc
Ionising flux	$4.8 \cdot 10^9 \text{ cm}^{-2} \text{ s}^{-1}$
Electronic surface density	720 cm^{-3}
Globule lifetime against photo-evaporation	10^6 yr
IRAS source position (1950)	$\alpha = 02^{\text{h}}25^{\text{m}}14.5^{\text{s}}$ $\delta = 61^{\circ}20'10''$ (1950)
IRAS fluxes	S(12,25,60,100 μm)= 9.81, 55.98, 239.51, 638.83 Jy
FIR luminosity	$1100 L_{\odot}$
Dust temperature (12 $\mu\text{m}/25 \mu\text{m}$)	135 K
Dust temperature (25 $\mu\text{m}/60 \mu\text{m}$)	68 K
Dust temperature (60 $\mu\text{m}/100 \mu\text{m}$)	32 K
Core gas temperature	40 K
Core density (peak)	$1.5 \cdot 10^6 \text{ cm}^{-3}$
Core density (average)	$2 \cdot 10^5 \text{ cm}^{-3}$
Core radius	0.08 pc
Core mass (C^{18}O , dust)	$21 M_{\odot}$
Envelope gas temperature	30 K
Envelope density (^{13}CO)	$4 \cdot 10^4 \text{ cm}^{-3}$
Envelope radius	0.3 pc
Envelope mass (^{13}CO)	$135 M_{\odot}$
Density structure	$\rho \propto r^{-1}$ in the range 0.1 – 0.2 pc.
Velocity structure	RDI motion on the southern side of the globule Bipolar Outflow centered on the IRAS source

7. Discussion

7.1. Dynamical interaction of CG5 with the UV flux

The outer contour of CG5 shown by the optical image, is a blunt cone, pointing at $\text{PA} \approx 80^{\circ}$, the radius of the head being $\approx 0.3 \text{ pc}$.

All the tracers of molecular gas, including high-density tracers such as CS(3-2) or CS(2-1) show the presence of an extended component of warmer gas along the southern border of CG5 (compare the ^{13}CO (2-1) maps of integrated emission and peak brightness in, respectively, Figs. 2 and 3). This layer is redshifted with respect to the main body gas. Inspection of the VLA map (see Fig. 1) shows that the morphology of the molecular layer is very similar to the region of maximum free-free emission (see Sect. 4.1).

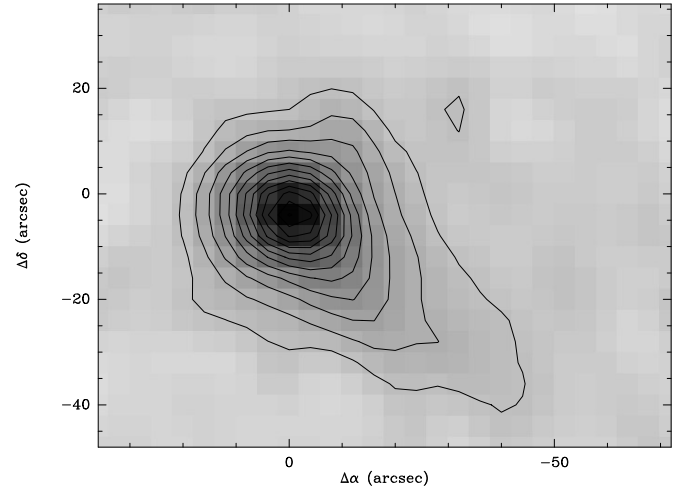


Fig. 12. Continuum emission map of CG5 at 1.25mm. First contour and contour step are 15 mJybeam^{-1} . The peak flux is 200 mJy/beam .

The most plausible explanation is that we actually observe the dense shocked gas ahead of the ionisation front at the surface of CG5. A simple calculation of the typical density n_s in this compressed layer (see Sect. 3.2) shows that it is comparable to the CS critical density.

As already mentioned in Sect. 2, the present distribution of ionized gas along the rim of CG5 does not follow the general symmetry of the globule and it seems likely that it acquired its shape in a previous photoevaporation episode. We propose that we are now observing a recompression of the south side of CG5 caused by the stars listed in Table 1 (essentially the last three).

Photo-ionisation of the superficial layers induces a mass loss of the cloud at a rate (LL94):

$$\begin{aligned} \dot{M} &= 29 \left(\frac{\Phi}{10^7 \text{ cm}^{-2} \text{ s}^{-1}} \right)^{1/2} \left(\frac{R}{1 \text{ pc}} \right)^{3/2} M_{\odot} \text{ My}^{-1} \\ &= 105 M_{\odot} \text{ My}^{-1} \end{aligned}$$

The lifetime of the molecular condensation τ_c is then $\tau_c \approx 1 \text{ My}$.

7.2. Pressures and magnetic field

The molecular density averaged over the cloud is: $n_c = 1.1 \cdot 10^4 \text{ cm}^{-3}$. Taking as mean linewidth $\Delta v = 2.1 \text{ km s}^{-1}$ and temperature $T = 30 \text{ K}$, we derive the thermal and turbulent pressure of the molecular gas:

$$P_{th} = 4.6 \cdot 10^{-11} \text{ erg cm}^{-3} \quad (10)$$

$$P_{turb} = 4.0 \cdot 10^{-10} \text{ erg cm}^{-3} \quad (11)$$

$$P_{ext} = 4.2 \cdot 10^{-9} \text{ erg cm}^{-3} \quad (12)$$

The dynamical pressure of the cloud therefore appears ten times as low as the external pressure. This is *qualitatively* correct since we actually have evidence of shock compression.

There is little doubt that the suprathermal linewidths observed are of magnetic origin (Alfvén, magnetosonic waves).

The energy contained in the magnetic field supporting these MHD waves provides support against collapse motions. Assuming that the Alfvénic Mach number M_A can be at most unity, because of the rapid rise of dissipation for higher values, we can write $\sigma_{turb}^2 \leq V_A^2/3 = B^2/(12\pi\rho)$, where $\sigma_{turb}^2 = 1/(8 \ln 2)\Delta V^2 - k_B T/m$ is the (1-d) non-thermal component of linewidths. Adopting the ^{13}CO estimates for σ_{turb} and ρ , we derive a lower limit for the magnetic field and its associated pressure:

$$B \geq 125 \mu\text{G} \quad (13)$$

An upper limit is obtained by assuming that a *static* magnetic field balances the outside pressure of the ionised gas: $B \leq 310 \mu\text{G}$. Because compression caused by P_{ext} is observed on the south rim, B must be significantly below the $310 \mu\text{G}$ upper limit and is probably closer to the $125 \mu\text{G}$ lower limit derived above. We therefore estimate the total magnetic (static plus MHD turbulent) pressure as: $P_B \approx 10^{-9} \text{ erg cm}^{-3}$.

Given the mean density of molecular gas in CG5, the strength of the magnetic field is compatible with the empirical Heiles' law, observed over a large range of scales in molecular clouds and HII regions $B/(1 \mu\text{G}) = A(n/1 \text{ cm}^{-3})^{1/2}$ where $A \sim 1.5$ with a fair amount of scatter (Heiles, 1993). The ratio of the inner (static magnetic plus MHD) pressure to the external pressure is $P_B/P_{ext} = 0.25$. Therefore, the magnetic energy present in the field and the MHD waves can support efficiently the cloud against the external pressure, and strongly slow down the implosion. From Mestel (1986), we estimate the maximum mass which can be supported against collapse by the magnetic flux $\Phi \approx \pi BR^2$: $M_c = 1/(3\pi^2 G)^{1/2} \Phi = 120 M_\odot$. CG5 is therefore in a marginally supercritical state with respect to the static magnetic field, and globally magnetically subcritical. We return to this point in the following section.

Can the bipolar outflow be the source of the turbulent energy? The timescale for the outflow mechanical power L to provide the observed turbulent energy can be estimated as: $\tau_{source} \approx 3P_{turb} < V > / (2L) = 0.1 \text{ My}$, while the dissipation timescale for near-sonic turbulence is of order of the sound crossing time: $\tau_{diss} \approx \ell/V_A = 0.3 \text{ pc}/1.5 \text{ km s}^{-1} \approx 0.2 \text{ My}$. Therefore, the outflow might be the source of the observed turbulent motions.

7.3. Gravitational stability and star formation

We first examine the virial balance of CG5 on large scales before concentrating on the properties of the molecular core. Leaving aside the compression region and the relatively small mass involved in the bipolar flow, CG5 appears to be in a quasi-static state and should obey the virial equation:

$$2T + \mathbf{M} - 3P_0V - |W| = 0 \quad (14)$$

Our observations do not allow us to evaluate the boundary pressure P_0 on the quiescent part of the surface of CG5. We can estimate the other terms in the virial equation, normalized to unit mass, in units of $(1 \text{ km s}^{-1})^2$: where the $2/3$ factor in $|W|$

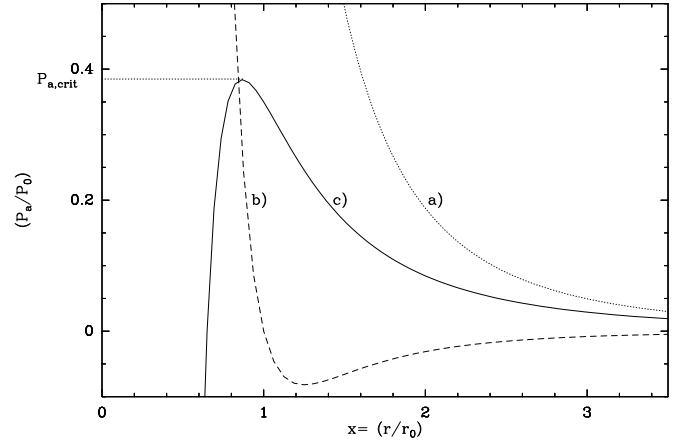


Fig. 13. Equilibrium states of a cloud sustained by its internal and a magnetic pressure against its self-gravity and an external pressure P_a . The cloud is in an arbitrary initial state (P_0, r_0) . The polytropic index of gas γ and the ratio of the non-kinetic to kinetic energy Λ define 3 possible configurations for the cloud (see text), illustrated here: a) $\Lambda > 0$, b) $\Lambda < 0$, $\gamma > 4/3$, and c) $\Lambda < 0$, $\gamma < 4/3$.

$3\sigma^2$	$B^2/(8\pi\rho)$	$3P_0/\rho$	$(2/3) \times 3GM/(5R)$
2.3	1.1	?	0.8

corresponds to a r^{-1} density distribution (see end of Sect. 6). The estimate of the first term is directly based on the observed velocity dispersion; the second term is a lower limit (if supersonic turbulence is excluded), and we estimate our mass determination (from the optically thin, thermalized $^{13}\text{CO}(1-0)$ line) to be accurate to 25% or better. We therefore conclude that *an external pressure $P_0 \approx 6 \cdot 10^{-10} \text{ erg cm}^{-3}$ is needed, together with self-gravity, to confine CG5.*

We now discuss the evolution leading to the present state of CG5. We propose the following scenario, that will be supported by a more quantitative analysis. The molecular condensation that became CG5 was, before being exposed to the UV flux of O stars, in a near-critical stability state. Photo-evaporation increased the surface pressure beyond a critical value, triggering the collapse of the central part and ensuing protostar formation. The present bipolar outflow(s) contribute to sustain turbulence and return the cloud to a globally subcritical state.

We present a simplified analysis based on the virial equation and isotropic contraction to determine the impact of an external pressure on the gravitational stability of a condensation such as CG5 for various initial conditions. We parametrize the contraction with $x = r/r_0$, where “0” denotes an arbitrary reference state, and assume that the gas pressure follows a polytropic equation of state $p = p_0(\rho/\rho_0)^\gamma$. We can then write the virial equation:

$$0 = 3P_0V_0x^{3(1-\gamma)} - 3P_ax^3 + \mathbf{M}_0x^{-1} - |W_0|x^{-1} \quad (15)$$

$$\frac{P_a}{P_0} = x^{-3\gamma} + \frac{\mathbf{M}_0 - |W_0|}{3P_0V_0}x^{-4} \quad (16)$$

Fig. 13 shows the qualitative behaviour of P_a versus x in three cases. An equilibrium state can exist for a given value of P_a

if the $P_a(x)$ curve intersects that ordinate; that equilibrium is stable is $dP_a/dx < 0$. Three cases arise:

a) $(\mathbf{M}_0 - |W_0|) > 0$: the magnetic pressure dominates gravity, and, irrespective of the gas equation of state, there is a stable equilibrium for arbitrary ambient pressure. This corresponds to a cloud for which the M/Φ ratio is subcritical.

b) $(\mathbf{M}_0 - |W_0|) < 0$, and $\gamma > 4/3$. Although the M/Φ ratio is supercritical, the stiffness of the equation of state guarantees a stable equilibrium for any ambient pressure. This includes the case of a magnetically supercritical collapse halted by adiabatic ($\gamma = 7/5$) pressure.

c) $(\mathbf{M}_0 - |W_0|) < 0$, and $\gamma < 4/3$. In that case, $P_a(x)$ goes through a maximum value $P_{a,crit}$. No equilibrium exists for $P_a > P_{a,crit}$.

In the special case $\gamma = 4/3$, the r.h.s. of Eq. 16 and its derivative have a sign which is independent of x , and the cloud is either unconditionally stable or unconditionally unstable (no curves are drawn on Fig. 13 for that case). The rest of the discussion depends on the effective γ for the dominant turbulent pressure, which is poorly known. If an alfvénic condition ($M_A = 1$) is maintained (possibly by balance between turbulent energy production and dissipation), then the effective γ is $4/3$. If, however, γ is less than $4/3$, either because of the contribution of the thermal pressure, or because of the behaviour of the turbulent pressure, then we are in case c).

All the condensations we observe now at the border or inside the HII region were (are still) very likely magnetically subcritical: supercritical condensations collapse in a few free-fall times $\tau_{ff}(= \sqrt{3\pi/(32G\rho)} = 3 \cdot 10^5 \text{ yr}$ for $n \sim 10^4 \text{ cm}^{-3}$), and would have already formed stars before being reached by the Ionisation Front. Ambipolar diffusion is a well established mechanism to drain magnetic flux outside molecular clouds and allow them to collapse (we will return to this point further down). Therefore, in a star-forming molecular complex, there must be at any time a number of cores close enough to the stability limit ($P_a = P_{a,crit}$) that the increase in boundary pressure due to photoionization pushes them over the top of the magnetic barrier.

Besides, using standard expressions (Mouschovias, 1991), we compute the ion density and ambipolar diffusion timescale in the central core of CG5 ($n(\text{H}_2) = 10^6 \text{ cm}^{-3}$):

$$n_i = 3 \cdot 10^{-3} \left(\frac{n(\text{H}_2)}{10^5} \right)^{1/2} = 10^{-2} \text{ cm}^{-3} \quad (17)$$

$$\tau_{AD} = 10^3 \frac{10^{10} n_i}{n(\text{H}_2)} \left(\frac{M}{M_C} \right)^2 \approx 10^5 \text{ yr} \quad (18)$$

where $M_C = (1/(63G))^{1/2} \Phi$ is the critical mass with respect to the magnetic flux. While the actual value of τ_{AD} might be higher due to ionisation of minor species (Fe, Si), the standard value is small enough with respect to the estimated lifetime of CG5 (10^6 yr) against dispersal by the UV flux that significant flux loss should also occur during the evolution of the cometary globule, so that the magnetic barrier could be passed *after* the start of the photo-ionisation.

The dynamics of the condensations in CG5 are governed by the three length scales: a) λ_A : the minimum Alfvén wave-

length which can propagate in the neutral gas, b) λ_T : the maximum length scale which can be supported against self-gravity by the cloud's kinetic pressure, c) λ_M : the maximum length scale which can be supported against self-gravity by the magnetic flux. They can be expressed as:

$$\lambda_A = 0.29 \left(\frac{B}{30 \mu\text{G}} \right) \left(\frac{10^3 \text{ cm}^{-3}}{n} \right) = 0.017 \text{ pc} \quad (19)$$

$$\lambda_T = 1.53 \left(\frac{\sigma}{1 \text{ km s}^{-1}} \right) \left(\frac{10^3 \text{ cm}^{-3}}{n} \right)^{1/2} = 0.10 \text{ pc} \quad (20)$$

$$\lambda_M = 0.91 \left(\frac{B}{30 \mu\text{G}} \right) \left(\frac{10^3 \text{ cm}^{-3}}{n} \right) = 0.056 \text{ pc} \quad (21)$$

where we have adopted the canonical values for the ionised fraction (Mouschovias, 1991). Numerical values are given for the parameters of the core of CG5 ($\Delta v = 1.3 \text{ km s}^{-1}$, $n(\text{H}_2) = 6.7 \cdot 10^4 \text{ cm}^{-3}$). λ_T is very close to the core radius ($= 0.095 \text{ pc}$), and larger than λ_M . This means that the core of CG5 is close to virial equilibrium and gravitationally bound (note that we have left aside the contribution to the gravitational potential of the protostars which might have formed in the core - see below).

The damping of Alfvén waves below the scale defined by λ_A results in a lower polytropic index γ for the gas at small-scales. Small-size condensations can therefore gravitationally collapse when they undergo the pressure increase P_a of the shock associated with the ionisation front, whereas the large-scale structures remain stable. Based on an energetic analysis, photo-ionisation appears to be a (if not "the") natural agent to trigger star formation in CG5. A more detailed modelling would be required to define an evolutionary scenario, including timescales.

What is the impact of the outflow on the core of CG5? In order to trigger the gravitational collapse of a gas condensation of mass m , the outflow momentum has to be greater than $m\sigma$, where σ is the typical linewidth in the condensation (0.55 km/s for the core of CG5) (Foster & Boss, 1996). The momentum contained in each lobe of the outflow is $< MV > \approx 5 M_\odot \text{ km s}^{-1}$. The outflow of CG5 is therefore able to trigger the gravitational collapse of condensations of mass $\leq 9 M_\odot$, leading to the formation of low- and intermediate-mass stars. We speculate that the outflow associated with the very first protostar might have induced or contributed to a sequential star-forming process in the cloud. On a large scale, the present outflow carries energy in the gas, which contributes to unbound the cloud. The external pressure exerted by photo-ionisation plays a key role in that it is the main agent to bind the cloud and oppose the gas dispersal favored by the energy injection of the outflow in the cloud (the virial analysis in Sect. 7.3 has shown that an external pressure is actually necessary to bind CG5). Thereby, star-formation inside CG5 indirectly contributes to slow down the collapse motion and lengthen the lifetime of the cloud, which in turn increases the number of protostars which can form. The counterpart is that the energy density of the molecular gas is higher; λ_T is increased and the objects formed are more massive, which in turn implies more

energy injected in the outflow, so that in the end the SFE is self-regulated.

7.4. Multiple star formation in CG5

Our observations show that star formation occurred recently in the molecular core of CG5: a CO molecular outflow associated to the central IRAS source has been observed; there is an almost exact coincidence between the nominal position of the IR source, the density peak of molecular gas, the peak of millimeter continuum emission and the apparent center of the outflow. However, the absence of an ultra-compact HII region in the core of CG5 and the examination of the equivalent 12μ IRAS flux at the distance of the Taurus complex $S_{12}^* = 1380 \text{ Jy}$ ($= S_{12} \cdot (d/160 \text{ pc})^2$) strongly suggests that *it is not a single object but a cluster of stars which has formed in CG5*. This is confirmed by IR observations made in the JHK bands by Skrutskie et al. (1990). The authors report the presence of a cluster of at least 20 sources in CG5. The luminosity of the cluster is dominated by a binary system, one of the stars being much younger (redder) than its companion. Taking as upper limit to the extent of the cluster the 30% contour of the $^{13}\text{CO}(1-0)$ integrated area, we derive (lower) estimates of 53 pc^{-2} for the stellar surface density and 160 pc^{-3} for the stellar density. The star forming efficiency of the globule (fraction of mass converted into stars) is more difficult to estimate since one has to take into account the mass of gas photo-evaporated. A rough estimate is obtained by assuming that half of the cloud mass has already been photo-evaporated and that all the stars formed have a typical mass of $1 M_{\odot}$; we obtain an efficiency of $\sim 10\%$. We conclude from these somewhat crude estimates that the star-forming properties of CG5 in the most conservative case are similar to those encountered in the ρ Oph core, where stars essentially form within clusters (Lada, Strom and Myers 1990).

A detailed analysis of the members of the star cluster (age, mass) from IR data would enable to precise the mass-spectrum and the star-forming efficiency of the cloud, especially with respect to the large star-forming complexes such as Orion or ρ Ophiuchus. Also, it probably is the best tool to validate our model of triggered star-formation: the stars formed closer to the surface of CG5 are expected to be older and should appear less red.

8. Conclusion

We have observed the cometary globule CG5 in the HII region IC 1848 at millimeter and centimeter wavelengths. Our study shows that this cloud is progressively emerging from the dense neutral gas layer surrounding the nebula. Comparison of the distribution of ionised gas along the cloud's rim and the general symmetry of the cloud suggests that CG5 acquired its shape in a previous episode of photo-evaporation by now-extinct stars. It is presently undergoing recompression of the south side by the O star cluster located at the center of the HII region. We estimate the UV flux $\Phi = 4.8 \cdot 10^9 \text{ cm}^{-2} \text{ s}^{-1}$ from the VLA free-free continuum emission at 6cm. The Ly-c photons of the exciting

stars of the nebula evaporate the superficial layers and drive a shock into the globule while the material at the surface of the cloud is heated: we estimate the shocked gas pressure to be $\approx 4\times$ as large as the inner pressure of the globule. The shocked gas in the compressed layer preceding the IF was detected in dense gas tracers and in the millimeter (thermal) emission of dust.

CG5 exhibits a strong resemblance with the barnacle models of LL94: it consists of a dense core ($M = 21 M_{\odot}$, $R = 0.08 \text{ pc}$) surrounded by a lower-density envelope of mean radius 0.3 pc . We found a total mass of $135 M_{\odot}$ for the whole cloud; the density distribution follows a $\rho \propto r^{-1}$ density law at least in the range $0.1 - 0.2 \text{ pc}$. A detailed analysis of pressure balance strongly supports the idea that the globule is permeated by a static magnetic field of strength close to $125 \mu\text{G}$, which also represents a lower limit assuming the observed linewidths are of Alfvénic origin, and less than $300 \mu\text{G}$. Consequently CG5 is globally *magnetically subcritical*. It is not self-gravity but the external overpressure resulting from photo-ionisation which confines the cloud, as a consequence of the star formation which took place inside the globule.

The luminous IRAS point source harboured in CG5 is the powering engine of a molecular outflow observed in different lines of the CO isotopomers and CS; this outflow is apparently very young ($T_d \sim 1.5 \cdot 10^4 \text{ yr}$) and entrains dense gas ($n \geq 3 \cdot 10^5 \text{ yr}$) of relatively high opacity. The source locally heats its parental core at a temperature $\approx 50 \text{ K}$. Both IRAS fluxes and IR observations lead to the conclusion that the source is multiple. Based on conservative estimates, the star-forming properties (stellar density, star-forming efficiency) seem similar to what is observed in the large star-forming complexes. At this point, IR observations combined with our data are needed to determine the mass spectrum and the star-forming efficiency of CG5, which might turn out to be even higher than our estimate.

We suggest that CG5 was in a magnetically subcritical state in the past, with some small-scale condensations close to critical equilibrium (we find e.g. the cloud core to be in virial equilibrium). The overpressure due to the shock driven by the ionisation front was then sufficient to trigger their gravitational collapse. The momentum contained in the outflow is also large enough that it might have contributed to this sequential star-formation process. In addition, the energy of the outflow is sufficient to sustain turbulence in the cloud and maintain it in a magnetically subcritical state, i.e. it tends to stabilize the cloud against collapse. It results that the SFE is self-regulated.

References

- Bachiller, R., Gómez-González, J., 1992, *Astron. Astrophys. Rev.*, 3, 257
- Bertoldi, F., 1989, *ApJ*, 346, 735
- Bertoldi, F., McKee, C., 1990, *ApJ*, 354, 529
- Cabrit, S., Bertout, C., 1990, *ApJ*, 348, 530
- Duvert, G., Cernicharo, J., Bachiller, R., Gómez-González, J., 1990, *A&A*, 233, 190
- Carpenter, J., Snell, R.L., Schloerb, F.P., Skrutskie, M.F., 1993, *ApJ*, 407, 657

- Deharveng, L., Zavagno, A., Cruz-González, I., Salas, L., Caplan, J., Carrasco, L., 1996, to appear in A&A
- Foster, P., Boss, A., 1996, ApJ, 468, 784
- Lada, E., Strom, K., and Myers, P.C., 1993, in Protostars and Planets III, Univ. of Arizona Press, Tucson & London
- Langer, W.D., Penzias, A.A., 1990, ApJ, 357, 477
- Lefloch, B., Lazareff, B., (LL94) 1994, A&A, 289, 559
- Lefloch, B., Lazareff, B., (LL95) 1995, A&A, 301, 552
- Lefloch, B., Lazareff, B., Castets, A., 1997, in prep.
- Mauesberger, R., Guélin, M., Martin-Pintado, J., Thum, C., Cernicharo, J., Hein, H., Navarro, S., 1989, A&A, 223, 376
- Mouschovias, T., 1991, in The Physics of Star Formation and Early Stellar Evolution (Ed: C.J. Lada & N.D. Kylafis), Kuwer Academic Publishers
- Mestel, in Protostars and Planets II, Univ. of Arizona Press, Tucson & London
- McKee, C.F.M., Zweibel, E.G., Goodman, A.A., Heiles, C., 1993, in Protostars and Planets III, Univ. of Arizona Press, Tucson & London
- Mezger, P.G., Wink, J.E., Zylka, R., 1990, A&A, 228, 95
- Mezger, P.G., Henderson, A.P., 1967, ApJ, 147, 471
- Neckel, T., Vehrenberg, H., 1985, Atlas of Galactic Nebulae, Treugesell-Verlag K.G. D-4000 Düsseldorf
- Panagia, N., 1973, As.J, 78, 929
- Reipurth, B., 1983, A&A, 117, 183
- Skrustkie, M.F., Meyer, M.R., Carrasco, L., Cruz-González, I., Salas, L., Johnson, P., Spillar, E., 1990, BAAS, 25, 1374
- Spitzer, L., 1978, Physical Processes in the Interstellar Medium, ed. John Wiley & Sons.
- Sugitani, K., Fukui, Y., Ogura, K., 1991, ApJ Supp., 77, 59
- Sugitani, K., Fukui, Y., Ogura, K., 1994, ApJ Supp., 92, 163
- Sugitani, K., Tamura, M., Ogura, K., 1995, ApJ, 455, L39